Data-Driven Identification and MPC of Coupled Tank System using Bilinear Koopman Realizations and Physics-Informed Neural Networks

Amir Vanegas, Julio Barón-Velandia, Nelson Leonardo Díaz-Aldana, and Duvan Tellez-Castro

***Abstract*— Real-time control of multivariable nonlinear processes requires models balancing high fidelity with computational tractability. This paper compares two data-driven paradigms: Bilinear Koopman Realizations and Physics-Informed Neural Networks. While standard Koopman approaches seek global linearization, we leverage a bilinear framework in the lifted functional space to preserve the natural coupling of control-affine systems. Simultaneously, PINNs ensure physical consistency by embedding conservation laws into the learning objective. To facilitate high-performance control, both surrogate models are integrated into a nonlinear model predictive control scheme using the CasADi framework, enabling efficient algorithmic differentiation for optimization. Simulation results for a quadruple tank system demonstrate that both paradigms reach mean VAF values above 99%, but the Bilinear Koopman model delivers a lower mean RMSE during step transients while doubling the computational speed of the PINN with a Real-Time Factor above 22. We conclude that despite structural scaling limitations regarding neural exploding gradients and operator instability risks, the Bilinear Koopman realization provides a more reliable, noise-resilient solution for real-time hydraulic benchmarks.**

***Index Terms*— Neural Networks, Nonlinear Optimization, Nonlinear Systems, Predictive Control, System Identification.**

I. INTRODUCTION

Real-time control of complex nonlinear processes requires models that balance accuracy with computational efficiency [1]. Traditional first-principles modeling often incurs high computational costs in online estimation and Model Predictive Control due to the recursive solution of differential equations [2]–[4]. To address these limitations, data-driven frameworks have emerged as a flexible alternative, capturing complex nonlinearities without relying on local linearization [3], [10]. Modern approaches, such as Bilinear Koopman Realizations and Physics-Informed Neural Networks, offer a scalable path for system identification by leveraging frameworks adaptable to increasing system dimensions. These methodologies provide high-fidelity alternatives, bypassing the extensive analytical redesign required by classical techniques as system complexity increases [6], [10], [12].

Within this context, the Koopman Operator provides a mathematical foundation for analyzing nonlinear dynamics by acting as an infinite-dimensional linear operator in the observables space [3], [5]. While traditional Extended Dynamic Mode Decomposition (EDMD) seeks linear lifting, recent advances emphasize Bilinear Koopman Realizations. As argued in [12], every control-affine system admits a bilinear realization in the lifted space, even when finite-dimensional linear representations fail. This framework enables structured control while preserving natural state-input coupling [2], [3]. However, despite their algebraic elegance, these purely data-driven approximations can struggle without enforced physical consistency, particularly under measurement uncertainty.

To mitigate these generalization and noise sensitivity issues, PINNs integrate differential equations as constraints into the loss function [6]. This architecture enables accurate system identification even with sparse datasets, as the model is forced to adhere to governing physical principles [4], [9]. The resulting synergy between deep learning and physics-based regularization enhances robustness against noise, overcoming the limitations of traditional black-box machine learning while maintaining the flexibility of data-driven methods [6], [9].

Whether physics-informed architectures outperform operator-theoretic methods in control-affine scenarios remains an open area. We bridge this gap by establishing a rigorous comparative analysis of Bilinear Koopman and PINN-based modeling for the identification and predictive control of the nonlinear quadruple tank system [7]. By embedding these models into an NMPC scheme via CasADi, we quantify the trade-offs between structure-aware operators and physics-regularized learning. Using multiple multi-seed simulation batches under stochastic noise for each scenario, our study assesses tracking accuracy and computational reliability through both standard performance metrics and statistical robustness comparisons, offering a reliable selection criterion for real-time control in complex hydraulic benchmarks with cross-coupled dynamics and square-root nonlinearities [2], [7].

The remainder of this paper is organized as follows: Section II provides mathematical preliminaries for MPC, Koopman Theory, and PINNs. Section III formalizes the quadruple tank dynamics and identification objectives. Section IV details the Bilinear Koopman and PINN methodology alongside the NMPC implementation. Section V presents the case study, including simulation results and comparative performance analysis. Finally, Section VI draws the concluding remarks.

II. PRELIMINARIES

This section formalizes MPC optimization, Koopman Operator, Bilinear Koopman Realizations and PINNs, establishing the mathematical foundation for system identification and control.

All authors are with Faculty of Engineering, Universidad Distrital Francisco José de Caldas, Bogotá D.C., Colombia {azvanegasc, jbaron, nldiaz, duatellezc,} @udistrital.edu.co

A. Model Predictive Control

MPC computes optimal control actions by solving a constrained optimization problem over a finite time horizon at each sampling instant k [2], [11]. Unlike traditional control laws, MPC leverages a surrogate model to predict the future evolution of the system, allowing the controller to anticipate complex dynamics and counteract disturbances before they affect the process.

The framework guides the system by minimizing a cost functional J over a prediction horizon N, which balances tracking performance, actuator effort, and smoothness

$$\min_{\mathbf{u}_0,\dots,\mathbf{u}_{N-1}} J = \sum_{i=0}^{N-1} \left(\|\hat{\mathbf{h}}_{k+i+1} - \mathbf{r}_{k+i+1}\|_{\mathbf{Q}}^2 + \|\mathbf{u}_i\|_{\mathbf{R}}^2 + \|\Delta\mathbf{u}_i\|_{\mathbf{R}_d}^2 \right).$$

This optimization is subject to the system dynamics and physical operational limits:

$$\begin{aligned} \hat{\mathbf{x}}_{i+1} &= f_{\text{model}}(\hat{\mathbf{x}}_i, \mathbf{u}_i), \quad \hat{\mathbf{x}}_0 = \mathbf{x}_k, \\ \mathbf{u}_{\min} &\le \mathbf{u}_i \le \mathbf{u}_{\max}, \\ \Delta\mathbf{u}_{\min} &\le \mathbf{u}_i - \mathbf{u}_{i-1} \le \Delta\mathbf{u}_{\max}, \end{aligned}$$

Where $\hat{\mathbf{h}}$ represents the predicted tank levels and $\mathbf{r}$ is the desired reference. The matrix $\mathbf{Q}$ defines the importance of tracking precision, $\mathbf{R}$ represents the penalty on energy consumption or control effort, and $\mathbf{R}_d$ accounts for the desire for temporal smoothness in the control signal. Since the controller's success depends entirely on the fidelity of the mapping f_{model}, this study evaluates the integration of Bilinear Koopman Realizations and Physics-Informed Neural Networks as the predictive engines within this optimization framework.

B. Koopman Operator Theory

Koopman operator theory provides a mathematical foundation for analyzing nonlinear dynamics by shifting the perspective from state-space trajectories to the evolution of functions. It describes nonlinear systems through an infinite-dimensional linear operator $\mathcal{K}$ that acts on a space of scalar-valued observables g, such that $\mathcal{K}g = g \circ \mathbf{f}$ [5]. In practice, this framework seeks to find a finite-dimensional *lifting* mapping $\mathbf{z} = \psi(\mathbf{h})$ that embeds the nonlinear manifold into a higher-dimensional space where the dynamics appear linear. However, while this linear lifting is mathematically elegant for autonomous systems, the introduction of external control inputs often breaks the global linearity, necessitating a more flexible representation to capture state-input interactions.

C. Bilinear Koopman Realizations

To bridge the gap between global linearization and control-affine systems, recent advances favor Bilinear Koopman Realizations over traditional linear approximations. As established in [12], every control-affine system admits a bilinear representation in the lifted functional space, even when a strictly linear one is unattainable. This approach approximates the dynamics by allowing the control input $\mathbf{u}$ to act multiplicatively with the lifted states $\mathbf{z}$

$$\mathbf{z}_{k+1} = \mathbf{A}\mathbf{z}_k + \sum_{j=1}^{m} (\mathbf{B}_j \mathbf{z}_k) u_{j,k} + \mathbf{D}\mathbf{u}_k.$$

Within this structure, $\mathbf{A}$ captures the autonomous drift, $\mathbf{B}_j$ represents state-input interactions, and $\mathbf{D}$ characterizes direct additive actuator effects. To recover physical variables, we identify an output matrix $\mathbf{C}$ via Ridge regression to satisfy $\hat{\mathbf{h}}_k = \mathbf{C}\mathbf{z}_k$. While this decomposition significantly improves prediction fidelity, the potential lack of physical consistency in purely data-driven mappings motivates the integration of physics-based constraints through neural architectures.

D. Physics-Informed Neural Networks

PINNs approximate dynamical system solutions by embedding governing physical equations directly into the network's optimization objective. The framework trains a neural network $\hat{\mathbf{h}}(t) = \mathcal{N}(t, \mathbf{v}; \boldsymbol{\theta})$ to represent system trajectories while strictly adhering to physical laws [4], [9]. A composite loss function $\mathcal{L}(\boldsymbol{\theta})$ governs the training process

$$\mathcal{L}(\boldsymbol{\theta}) = w_d \mathcal{L}_{data} + w_p \mathcal{L}_{phys} + w_{ic} \mathcal{L}_{ic}, \tag{1}$$

where weighting coefficients w_i balance each term's contribution. Specifically, $\mathcal{L}_{data}$ quantifies the mean squared error against measured data, while $\mathcal{L}_{ic}$ enforces initial conditions. To maintain physical consistency, the residual term $\mathcal{L}_{phys}$ leverages automatic differentiation to evaluate the governing law:

$$\mathbf{r}(t) = \frac{d}{dt}\hat{\mathbf{h}}(t) - \mathbf{f}(\hat{\mathbf{h}}(t), \mathbf{v}(t); \omega).$$

By minimizing the norm of this residual over collocation points, the network converges toward a solution that satisfies fundamental physics principles. This approach effectively bridges the gap between purely data-driven methods and first-principles modeling.

III. PROBLEM FORMULATION

This section establishes the mathematical foundation of the quadruple tank system and formalizes the data-driven identification and control objectives addressed in this study.

A. Quadruple Tank System Dynamics

The quadruple-tank process serves as a multivariable (MIMO) benchmark for control, characterized by complex cross-coupled dynamics. As Fig. 1 illustrates, the setup utilizes two pumps to distribute flow among four interconnected tanks through a specific valve configuration. Mass conservation and Bernoulli's principle define the following nonlinear state-space representation:

$$\begin{aligned} \dot{h}_1 &= -\frac{a_1}{A_1}\sqrt{2gh_1} + \frac{a_3}{A_1}\sqrt{2gh_3} + \frac{\gamma_1 k_1}{A_1} v_1, \\ \dot{h}_2 &= -\frac{a_2}{A_2}\sqrt{2gh_2} + \frac{a_4}{A_2}\sqrt{2gh_4} + \frac{\gamma_2 k_2}{A_2} v_2, \\ \dot{h}_3 &= -\frac{a_3}{A_3}\sqrt{2gh_3} + \frac{(1-\gamma_2) k_2}{A_3} v_2, \\ \dot{h}_4 &= -\frac{a_4}{A_4}\sqrt{2gh_4} + \frac{(1-\gamma_1) k_1}{A_4} v_1, \end{aligned}$$

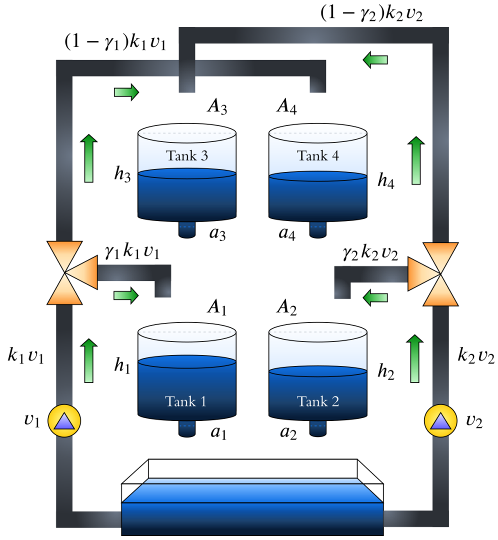

Fig. 1. Quadruple Tank System Representation.

where h_i represents the water level in each tank and v_i denotes the pump voltages. The parameters A_i and a_i correspond to the cross-sectional and outlet areas, respectively; k_i are the flow constants, and $\gamma_1, \gamma_2 \in [0,1]$ represent the valve settings that determine the flow distribution. The system output vector $\mathbf{y}$ collects the measured levels of all four tanks:

$$\mathbf{y} = [h_1, h_2, h_3, h_4]^\top.$$

Torricelli's Law introduces square-root nonlinearities, while the system equations reveal strong cross-coupling; specifically, the levels h_3 and h_4 directly drive the dynamics of the lower tanks. These structural interdependencies demand high-fidelity identification to achieve effective regulation within the control framework [2], [7].

B. Identification and Control Objectives

This work primarily aims to identify accurate surrogate models for the quadruple tank system using two distinct data-driven paradigms: Bilinear Koopman Realizations and PINNs. These models must capture nonlinear interactions and cross-coupling effects to enable precise trajectory tracking. Consequently, the control problem involves designing an MPC strategy to regulate the lower tank levels (h_1, h_2) by manipulating pump voltages $\mathbf{v} = [v_1, v_2]^\top$.

IV. Methodology

This section details the data-driven identification strategy and the MPC framework designed to regulate the quadruple tank's nonlinear cross-coupled dynamics.

A. Bilinear Koopman Identification

The identification process implements the transition function f_{model} by mapping tank levels $\mathbf{h} \in \mathbb{R}^4$ into a higher-dimensional feature space. To capture Bernoulli-driven nonlinearities and trigonometric couplings, we employ the dictionary

$$\mathbf{z} = \boldsymbol{\psi}(\mathbf{h}) = [\mathbf{h}, \sqrt{|\mathbf{h}|}, \sin(\mathbf{h}), \cos(\mathbf{h}), \mathbf{h}^2, |\mathbf{h}|, \boldsymbol{\phi}_{\text{RBF}}(\mathbf{h})]^\top,$$

where the Radial Basis Function vector $\boldsymbol{\phi}_{\text{RBF}}(\mathbf{h}) = [\phi_1(\mathbf{h}), \dots, \phi_M(\mathbf{h})]^\top \in \mathbb{R}^M$ computes each element via $\phi_j(\mathbf{h}) = \exp(-\|\mathbf{h} - \mathbf{c}_j\|^2/\sigma)$ relative to the centers $\mathbf{c}_j$.

$$\min_{\mathbf{W}_{\text{dyn}}} \|\mathbf{Z}_{\text{next}} - \mathbf{W}_{\text{dyn}}\mathbf{X}_{\text{reg}}\|_F^2 + \alpha_1 \|\mathbf{W}_{\text{dyn}}\|_F^2,$$

To identify the operator matrices, we construct a regression matrix $\mathbf{X}_{\text{reg}}$ containing the lifted states $\mathbf{z}_k$, the control inputs $\mathbf{u}_k$, and their bilinear interactions $\mathbf{z}_k u_{j,k}$. The weights for the dynamical evolution $\mathbf{W}_{\text{dyn}} = [\mathbf{A}, \mathbf{B}_1, \dots, \mathbf{B}_m, \mathbf{D}]$ are estimated via Ridge regression

$$\min_{\mathbf{W}_{\text{dyn}}} \|\mathbf{Z}_{\text{next}} - \mathbf{W}_{\text{dyn}}\mathbf{X}_{\text{reg}}\|_F^2 + \alpha_1 \|\mathbf{W}_{\text{dyn}}\|_F^2,$$

where α_1 ensures numerical stability against sensor noise and F denotes the Frobenius norm. Subsequently, we identify the output matrix $\mathbf{C}$ by solving a separate regularized least-squares problem

$$\min_{\mathbf{C}} \|\mathbf{H} - \mathbf{C}\mathbf{Z}\|_F^2 + \alpha_2 \|\mathbf{C}\|_F^2,$$

using the full dataset. This two-step identification allows the NMPC to evolve the system state within the lifted manifold while maintaining a precise, high-fidelity projection back to the physical level measurements.

B. PINN Identification

As an alternative, a PINN identifier approximates the function f_{model} through a deep residual network $\mathcal{N}$. The architecture processes the input vector $[\mathbf{x}_k, \mathbf{u}_k] \in \mathbb{R}^6$ to predict the subsequent state $\hat{\mathbf{x}}_{k+1}$. To enforce physical consistency, the training process minimizes the composite loss in (1), where the residual term $\mathcal{L}_{res}$ penalizes deviations from the discrete-time mass balance

$$\mathbf{R}_k = \hat{\mathbf{x}}_{k+1} - \left(\mathbf{x}_k + \Delta t \cdot \mathbf{f}_{phys}(\mathbf{x}_k, \mathbf{u}_k)\right).$$

To maintain numerical stability, f_{model} utilizes a scaling mapping based on the training extrema $[h_{\min}, h_{\max}]$. This normalization, in conjunction with optimization clipping, restricts the predicted trajectories $\hat{\mathbf{x}}$ to the feasible hydraulic range during MPC execution.

C. MPC Approach

The proposed framework utilizes a NMPC strategy centered on the CasADi suite. By leveraging algorithmic differentiation, the controller transforms the surrogate models f_{model} into differentiable expressions for high-performance gradient-based solvers.

Both configurations solve the optimization via Sequential Quadratic Programming using qpOASES, handling the bilinear and neural dynamics through successive linearizations. To enforce real-time feasibility, both implementations execute a warm-start strategy using the previous control sequence $\mathbf{u}^*_{k-1}$. This unified approach ensures that performance differences stem strictly from the predictive fidelity of the underlying data-driven paradigms rather than discrepancies in the optimization pipeline.

V. CASE STUDY

This section details the implemented environment, the training protocol for neural surrogates, and the physical parameters of the quadruple tank benchmark.

A. System Parameters

Plant simulation and predictive models rely on the geometric and flow constants from the Johansson benchmark [7], summarized in Table I. These values define minimum phase characteristics and the multivariable coupling strength of the system.

TABLE I
PHYSICAL PARAMETERS OF THE QUADRUPLE TANK SYSTEM.

Symbol	Description	Value	Unit
$A_{1,3}$	Area (Tanks 1 & 3)	28.00	cm^2
$A_{2,4}$	Area (Tanks 2 & 4)	32.00	cm^2
$a_{1,3}$	Outlet area (Tanks 1 & 3)	0.071	cm^2
$a_{2,4}$	Outlet area (Tanks 2 & 4)	0.057	cm^2
k_1, k_2	Pump flow constants	3.33, 3.35	cm^3/Vs
γ_1, γ_2	Flow split ratios	0.70, 0.60	–
g	Gravity	981.00	cm/s^2

B. Data Acquisition and Excitation

To achieve persistent excitation, data collection spans 5000 s with a sampling period $dt = 0.05$ s. A 4th-order Runge-Kutta method (RK45) solves the nonlinear plant from initial conditions $\mathbf{h}_0 = [12.4, 12.7, 1.8, 1.4]^\top$ cm.

Excitation signals $\mathbf{u} = [v_1, v_2]^\top$ consist of a Pseudo-Random Binary Sequence (PRBS) within $[0, 6]$ V, switching every 50 s. Reproducibility is ensured via a Mersenne Twister (MT19937) generator with a fixed seed of 100. Furthermore, to emulate realistic conditions, additive white Gaussian noise (AWGN) with $\sigma = 0.1$ affects both control inputs and output measurements.

C. Identification Parameters and Training

The framework implements the PINN using Python and *PyTorch*, accelerating operations via an *NVIDIA GeForce GTX 1050 Mobile* GPU and *Intel Core i5-8300H* CPU. To configure both models, we employed the *Optuna* framework to select the specific hyperparameters detailed in Table II. Before training, a Kalman filter with covariance matrices $\mathbf{Q} = 10^{-5}\mathbf{I}$ and $\mathbf{R} = 10^{-2}\mathbf{I}$ processes the raw simulation data to mitigate measurement noise. While the Bilinear Koopman model operates directly on these filtered scales to preserve structural mapping, the PINN framework subsequently normalizes the measurements to $[0, 1]$ to ensure numerical stability and faster convergence. For the neural architecture, training utilizes a dual-phase strategy: an Adam optimizer performs the global search, followed by L-BFGS for second-order refinement of physical residuals.

TABLE II
PARAMETERS FOR KOOPMAN AND PINN IDENTIFICATION

Koopman Parameter	Value	PINN Parameter	Value
Observables (n_{obs})	32	Hidden Layers	4
Regularization (λ)	8.8×10^{-7}	Neurons per Layer	48
RBF bandwidth (σ)	20	Activation Function	SiLU
RBF centers count (M)	8	Adam Epochs	4000
$\mathbf{K}$ matrix size	4×32	L-BFGS Max Iter.	4000

D. Identification Results

Multi-step prediction evaluation compares Bilinear Koopman and PINN trajectories against a State-space linearization, a standard Linear Koopman model, and actual tank levels. Fig. 2 illustrates this comparison over a validation window (2500–5000 s). Both the Bilinear Koopman model and the PINN capture the system nonlinearities with high structural fidelity and minimal deviation from the ground truth. While the State-space and Linear Koopman approximations provide a reasonable baseline, they exhibit a noticeable drift in highly nonlinear regions.

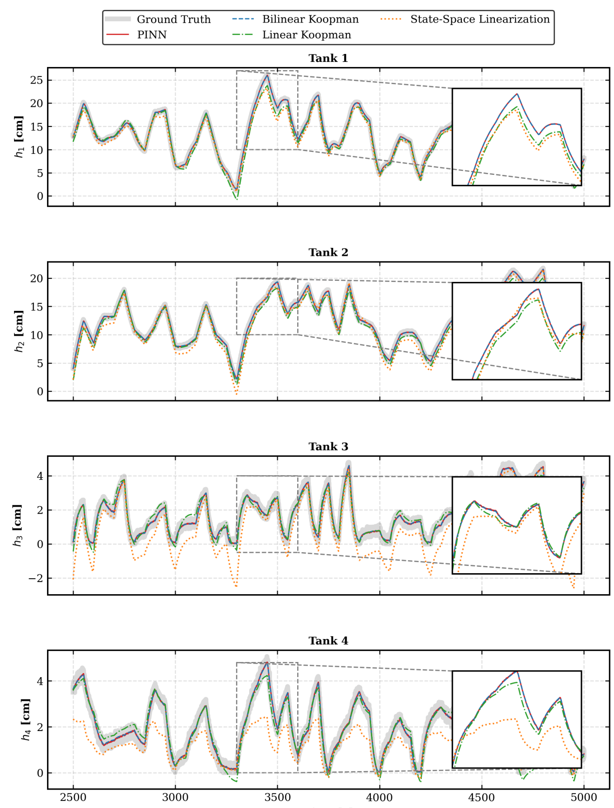

Fig. 2. Identification results: Bilinear Koopman vs Linear Koopman vs PINN vs State-space Linearization.

E. Model Validation Metrics

Quantitative assessment reveals that both Bilinear Koopman and PINN architectures achieve exceptional fidelity, consistently reaching VAF values above 99% across all tanks. As shown in Table III, these models significantly outperform

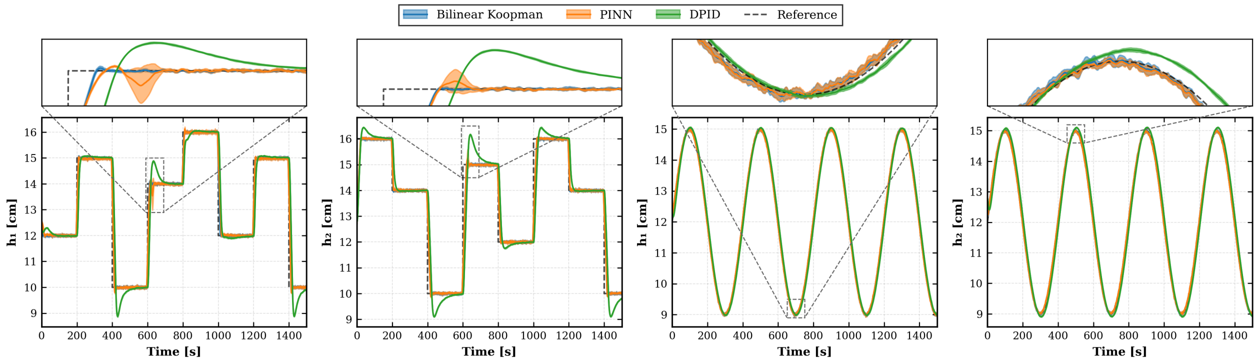

Fig. 3. Control performance comparison between NMPC-Bilinear Koopman, MPC-PINN and DPID: Sinusoidal Tracking and Step Response Cascade.

Linear Koopman and State-space Linearization baselines, which exhibit substantial degradation in the upper stages. This gap underscores the necessity of nonlinear lifting or physical regularization to capture complex hydraulic couplings.

While both methods demonstrate near-identical accuracy, the Bilinear Koopman realization slightly leads in h_3 and h_4 by exploiting the natural control-affine structure. These results confirm that embedding system knowledge provides a robust representation superior to traditional local approximations.

TABLE III
DETAILED PREDICTION METRICS PER TANK.

Model	Tank	RMSE (cm)	VAF (%)
PINN	h_1	**0.2061**	**99.85**
	h_2	0.1770	**99.83**
	h_3	0.1228	99.06
	h_4	0.1125	99.03
Bilinear Koopman	h_1	0.2107	99.84
	h_2	**0.1764**	**99.83**
	h_3	**0.1222**	**99.07**
	h_4	**0.1114**	**99.05**
Linear Koopman	h_1	0.8986	98.35
	h_2	0.7192	98.75
	h_3	0.3322	93.25
	h_4	0.2543	95.28
State-space Linearization	h_1	1.3188	96.24
	h_2	1.2000	96.59
	h_3	1.1826	59.26
	h_4	0.8995	75.24

F. Controller Real-Time Execution and Feedback Loop

The NMPC operates in a closed-loop with a sampling period of $\Delta t = 1$ s. At each step, the controller receives filtered measurements and computes the optimal sequence using a warm-start strategy from $\mathbf{u}^*_{k-1}$. Robustness is verified by injecting AWGN into sensors ($\sigma = 0.1$) and actuators ($\sigma = 0.15$), evaluating resilience to stochastic disturbances.

Table IV summarizes the NMPC hyperparameters used for both predictive models. The weighting matrices prioritize tracking accuracy in the lower tanks ($\mathbf{Q}$) while ensuring control effort economy ($\mathbf{R}$) and actuator smoothness ($\mathbf{R}_d$).

TABLE IV
NMPC HYPERPARAMETERS

Parameter	Value	Description
N_p	25	Prediction horizon [steps]
N_c	1	Control horizon [steps]
$\Delta\mathbf{u}_{\max}$	0.5	Slew-rate limit [V]
Weighting Matrices		
$q_{1,2}$	500	Tracking weights (h_1, h_2)
$q_{3,4}$	0	Stability weights (h_3, h_4)
$\mathbf{R}$	$0.01 \cdot \mathbf{I}$	Control effort weight
$\mathbf{R}_d$	$1.0 \cdot \mathbf{I}$	Slew-rate weight

G. Control Scenarios and Tracking Performance

To evaluate the agility and robustness of the proposed predictors, we execute 10 closed-loop simulations per model, varying the random seed across a 1500 s horizon with a sampling period of $\Delta t = 0.2$ s. The first scenario employs a Step Response Cascade where h_1 and h_2 alternate between 12, 15, 10, 14, and 16 cm every 200 s to quantify transient handling and settling time. Subsequently, a MIMO Sinusoidal Tracking scenario stresses the multivariable couplings through the reference $\mathbf{r}(t) = 12.0 + 3.0 \sin(2\pi t/400)$, assessing how accurately the data-driven models capture the nonlinear oscillations of the quadruple tank system.

H. Control Performance Analysis

Fig. 3 compares closed-loop tracking alongside standard deviation shaded areas. Both data-driven NMPC schemes significantly outperform the decentralized PID (DPID) baseline, which exhibits severe overshoots and slow settling times due to multivariable couplings. During transients, the Bilinear Koopman NMPC demonstrates superior statistical robustness over the PINN. As the close-ups highlight, the PINN yields wider deviation bands and oscillatory artifacts under stochastic noise. Conversely, the Bilinear Koopman realization maintains tight tracking bounds, confirming that its control-affine structure filters high-frequency disturbances more effectively.

I. Control Validation Metrics

Table V summarizes the global error analysis for both scenarios. Both data-driven controllers significantly outperform

TABLE V

GLOBAL PERFORMANCE METRICS FOR MPC COMPARISON.

Scenario	Metric	Unit	Bilinear Koopman			PINN			DPID		
			Mean	Std	99% CI	Mean	Std	99% CI	Mean	Std	99% CI
Sinusoidal Tracking	RMSE	cm	**0.0955**	0.0012	(0.0943, 0.0968)	**0.0955**	0.0011	(0.0944, 0.0966)	0.1207	0.0006	(0.1201, 0.1213)
	NRMSE	-	**0.0159**	0.0002	(0.0157, 0.0161)	**0.0159**	0.0002	(0.0157, 0.0161)	0.0201	0.0001	(0.0200, 0.0202)
	ISE	cm^2s	**27.382**	0.7067	(26.656, 28.109)	27.444	**0.5943**	(26.833, 28.054)	47.787	0.4529	(47.321, 48.252)
	RTF	-	**22.38**	0.6957	(21.67, 23.10)	10.68	0.2861	(10.39, 10.98)	9.51	0.2093	(9.29, 9.72)
Step Response Cascade	RMSE	cm	**0.4403**	0.0040	(0.4362, 0.4445)	0.4528	0.0061	(0.4465, 0.4590)	0.8224	0.0031	(0.8192, 0.8256)
	NRMSE	-	**0.0734**	0.0007	(0.0727, 0.0741)	0.0755	0.0010	(0.0744, 0.0765)	0.1371	0.0005	(0.1365, 0.1376)
	ISE	cm^2s	**595.84**	10.761	(584.79, 606.90)	624.28	15.697	(608.15, 640.41)	2032.3	15.161	(2016.7, 2047.9)
	RTF	-	**23.24**	1.1716	(22.03, 24.44)	10.78	0.0633	(10.71, 10.84)	10.24	0.3143	(9.91, 10.56)

Note: Calculations derive the 99% confidence intervals (CI) using a Student's t-distribution based on a sample size of $n = 10$ stochastic simulations.

the DPID baseline, which yields the highest tracking errors and lowest computational efficiency. In the Sinusoidal Tracking scenario, the Bilinear Koopman and PINN frameworks achieve identical mean RMSE values (0.0955 cm), though Koopman minimizes the Integral Squared Error (ISE) further. For the Step Response Cascade, the Bilinear Koopman NMPC firmly establishes its superiority, delivering lower mean RMSE (0.4403 cm) and reduced variance compared to the PINN.

Furthermore, the Bilinear Koopman model achieves a Real-Time Factor (RTF) above 22, doubling the execution speed of both the PINN and DPID. This computational advantage highlights the efficiency of the uncoupled control-affine formulation for optimization within the SQP pipeline, avoiding the heavy internal layers evaluation inherent to deep neural architectures.

VI. CONCLUSION

This study evaluated Bilinear Koopman and PINN architectures for the NMPC of a nonlinear quadruple tank system. Quantitative results demonstrate that both data-driven paradigms achieve high structural fidelity, reaching mean VAF values above 99%. However, the Bilinear Koopman framework effectively filters high-frequency disturbances, maintaining narrower standard deviation bands and tighter tracking bounds than the noise-sensitive PINN. Within the SQP pipeline, the Koopman NMPC firmly establishes superiority during step transients by delivering a lower mean RMSE and a Real-Time Factor above 22, doubling the computational speed of the neural approach.

While these results validate real-time feasibility, scaling to higher-dimensional networks exposes critical structural limitations. For the PINN, increased data complexity exacerbates vulnerability to exploding gradients during training. Conversely, the Bilinear Koopman realization suffers from severe instability risks as lifting dimensions expand, making it difficult to prevent eigenvalues from crossing the unit circle. Future work will address these constraints by exploring sparse identification and robust stabilization constraints under broader operational regimes.

DATA AND CODE AVAILABILITY

The source code, simulation results, and models used in this study are available to support reproducibility. These resources include the implementation of the PINN, Bilinear Koopman Realization, and NMPC architectures. Access the repository at: `https://github.com/azvcud/CoDiT_Comparison-of-PINN-and-Bilinear-Koopman`.

REFERENCES

[1] A. Annaswamy, K. H. Johansson, and G. J. P., eds., "Control for Societal-Scale Challenges: Road Map 2030," IEEE Control Systems Society, 2023.

[2] D. Santiago Aponte and D. Tellez-Castro, "Koopman-Based MPC for the Quadruple Tank System: An Experimental Comparison," in *2025 IEEE 7th Colombian Conference on Automatic Control (CCAC)*, pp. 1–6, 2025.

[3] M. Korda and I. Mezić, "Linear predictors for nonlinear dynamical systems: Koopman operator meets model predictive control," *Automatica*, vol. 93, pp. 149–160, 2018.

[4] R. Patel, S. Bhartiya, and R. Gudi, "Model Predictive Control using Physics Informed Neural Networks for Process Systems," *IFAC-PapersOnLine*, vol. 58, no. 14, pp. 775–780, 2024.

[5] B. O. Koopman, "Hamiltonian systems and transformation in Hilbert space," *Proc. Natl. Acad. Sci. U.S.A.*, vol. 17, no. 5, 1931.

[6] M. Raissi, P. Perdikaris, and G. E. Karniadakis, "Physics-informed neural networks: A deep learning framework for solving forward and inverse problems involving nonlinear partial differential equations," *Journal of Computational Physics*, vol. 378, pp. 686–707, 2019.

[7] K. H. Johansson, "The quadruple-tank process: A multivariable laboratory process with an adjustable zero," *IEEE Trans. Control Syst. Technol.*, vol. 8, no. 3, pp. 456–465, 2000.

[8] Y. Zuo, C. Yang, S. Li, W. Wang, C. Xiang, and T. Qie, "A model predictive trajectory tracking control strategy for heavy-duty unmanned tracked vehicle using deep Koopman operator," *Engineering Applications of Artificial Intelligence*, vol. 159, p. 111698, 2025.

[9] D. Chen, C.-K. Chui, and P. S. Lee, "Physics informed machine learning based predictive control for intelligent operation of edge datacenters," *Applied Energy*, vol. 402, Art. no. 126975, 2026.

[10] A. Taghieh, E. Cibaku, and S. Park, "Learning Koopman Observables via Kolmogorov-Arnold Networks for Power System Transient Analysis and Model Predictive Control," in *2025 IEEE 64th Conference on Decision and Control (CDC)*, pp. 387–394, 2025.

[11] J. A. E. Andersson, J. Gillis, G. Horn, J. B. Rawlings, and M. Diehl, "CasADi – A software framework for nonlinear optimization and optimal control," *Mathematical Programming Computation*, vol. 11, no. 1, pp. 1–36, 2019.

[12] D. Bruder, X. Fu, and R. Vasudevan, "Advantages of bilinear Koopman realizations for the modeling and control of systems with unknown dynamics," *IEEE Robotics and Automation Letters*, vol. 6, pp. 4369–4376, 2020.